STRUCTURE-FUNCTION RELATIONSHIPS OF MUCOCILIARY CLEARANCE IN HUMAN AIRWAYS

Doris Roth[1,2†], Ayşe Tuğçe Şahin[1,2†], Feng Ling[1,2,4], Christiana N. Senger[3], Erik J. Quiroz[3,5], Ben A. Calvert[3,5], Anne van der Does[6], Tankut G. Güney[1,2], Niels Tepho[1,2], Sarah Glasl[1,2], Annemarie van Schadewijk[6], Laura von Schledorn[7,8,9], Ruth Olmer[7,8,9], Eva Kanso[4], Janna C. Nawroth[1,2,3,4#*], Amy L. Ryan[3,5,10#*]

[1]   Helmholtz Pioneer Campus and Institute of Biological and Medical Imaging, Helmholtz Zentrum München, Neuherberg, D-85764, Germany

[2]   Chair of Biological Imaging at the Central Institute for Translational Cancer Research (TranslaTUM), School of Medicine, Technical University of Munich, Munich, D-81675, Germany

[3]   Hastings Center for Pulmonary Research, Division of Pulmonary, Critical Care and Sleep Medicine, Department of Medicine, University of Southern California, Los Angeles, CA

[4]   Department of Aerospace and Mechanical Engineering, University of Southern California, Los Angeles, California 90089, USA

[5]   Department of Stem Cell Biology and Regenerative Medicine, University of Southern California, Los Angeles, CA

[6]   PulmoScience Lab, Department of Pulmonology, Leiden University Medical Center, Leiden, the Netherlands

[7]   Leibniz Research Laboratories for Biotechnology and Artificial Organs (LEBAO), Department of Cardiothoracic, Transplantation and Vascular Surgery (HTTG), Hannover Medical School, 30625 Hannover, Germany

[8]   Biomedical Research in Endstage and Obstructive Lung Disease (BREATH), Member of the German Center for Lung Research (DZL), Hannover Medical School, 30625 Hannover, Germany.

[9]   REBIRTH-Research Center for Translational and Regenerative Medicine, Hannover Medical School, 30625 Hannover, Germany.

[10]   Department of Anatomy and Cell Biology, Carver College of Medicine, University of Iowa, IA

[†,#] These authors contributed equally to this manuscript

*Co-corresponding authors

Amy L. Ryan, PhD
Associate Professor: Anatomy and Cell Biology
Associate Director: Center for Gene Therapy
BSB, 1-400 Core
University of Iowa
51 Newton Road
Iowa City, Iowa, 52242
Email: amy-l-ryan@uiowa.edu
Tel: +1 319 335 8908

Janna C. Nawroth, PhD
Principal Investigator: Helmholtz Pioneer Campus
TUM Junior Fellow: Technical University of Munich
Deutsches Forschungszentrum fuer Gesundheit und Umwelt (GmbH),

Ingolstaedter Landstrasse 1, 85764 Neuherberg, Germany
Email: janna.nawroth@helmholtz-munich.de
Tel: +49 89 4140 9018

AUTHOR CONTRIBUTIONS

ABSTRACT

Mucociliary clearance (MCC) is a key mechanical defense mechanism of the human airways, and MCC failure is linked to major respiratory diseases. While single-cell transcriptomics have unveiled the cellular complexity of the human airway epithelium, our insights into the mechanical structure-function relationships that drive MCC mainly stem from animal models, limiting our understanding and *in vitro* modeling of human airway barrier function and disease. This study addresses these knowledge gaps and (1) reveals key differences in abundance and proportion of ciliated and secretory cell types at the luminal surface along the proximo-distal axis of the human and rat airway epithelium, (2) identifies ciliary beat properties that vary between species, and (3) quantitatively links these structural differences to differences in particle clearance function using a combination of experimental approaches and physics-based modeling. Finally, we leverage these structure-function relationships to develop metrics of organotypic tissue composition and clearance function in human airway epithelia, leading to the establishment of human-specific benchmarks for *in vitro* respiratory cultures, and allowing us to quantitatively compare the mucociliary machinery of different model systems, *in vitro* culture conditions, and disease states.

INTRODUCTION

Mucociliary clearance (MCC) is a critical mechanical defense and barrier mechanism of the human airways[1–4]. In MCC, a layer of mucus is continuously swept across the epithelial surface, thereby removing inhaled particles and pathogens. Specialized multiciliated cells propel the mucus, a mixture generated by a variety of secretory cells, including mucin-secreting goblet cells, surfactant-secreting club cells, and their intermediate stages[1,2,5–7]. Failure of MCC contributes to the debilitating pathophysiology of many respiratory diseases, including chronic obstructive pulmonary disease (COPD), primary ciliary dyskinesia (PCD), asthma, and cystic fibrosis (CF)[8]. However, our understanding of impaired MCC in disease remains limited by our incomplete knowledge of the mechanical structure-function relationships of MCC in humans[4] since most studies use animal models[9]. Data on live ciliary beat and clearance function are challenging to obtain in humans and remain rare in literature[10]. Luminal cellular organization remains equally understudied since conventional histology best reveals cross-sectional, instead of luminal, tissue architecture. Transcriptional profiling commonly does not resolve spatial organization[11] and is not guaranteed to correspond to protein expression[12].

The lack of such data limits our understanding and modeling of human MCC. For example, a recent study showed that while luminal surface ciliation in mouse trachea is relatively low (approximately 40%), the specific distribution and orientation of ciliary beat nonetheless confers robust and efficient particle clearance[13]. The authors could only speculate that these design rules may directly translate to humans as well, where such quantitative insights could help refine treatment targets for diseases that impair ciliary beat, such as primary ciliary dyskinesia[14], or cause the loss of ciliated cells, such as asthma[15]. Limited human-relevancy of animal studies have led to the rise of innovative *in vitro* human airway epithelial models[16–18]. But without quantitative benchmarks describing normal clearance function in humans, the ability of these models to accurately represent airway barrier function and dysfunction remains unknown. Lastly, the proportion of ciliated and different secretory cell types is thought to differ along the airway tree in humans and rats[19]. It remains unclear whether this results in regional differences in MCC and whether diseases that alter the proportions of airway epithelial cell types[20] have differential functional impact dependent upon the region of the airways[4].

Here, we address these knowledge gaps by (1) creating a quantitative map of the luminal distribution of ciliated, club and goblet cells and the associated particle clearance function along the proximal-distal axis of the human and rat airway tree, (2) developing quantitative metrics and physics-based computational models that capture key characteristics and structure-function relationships of MCC in airway epithelia, and (3) using these metrics for assessing the structural and functional similarity of *in vitro* human airway epithelial cultures generated in a variety of cell culture conditions to native airway epithelia.

RESULTS

Tracheo-bronchial ciliation is significantly different between human and rat airways.

We measured live ciliary beat and particle clearance[10,21] in freshly isolated airway epithelial tissue from respiratory tree branching generation (BG) 0 through BG6 from 3 human whole lungs with no prior history of chronic lung disease, and BG0 through BG5 from healthy rat whole lungs (**Fig. 1a;** for detailed donor information and numbers used in subsequent results see **Supplementary Tables S1 & S2).** Subsequently, we determined the airway diameter (**Supplementary Figure S1**) and quantified the luminal cell type composition in these samples and additional human bronchial rings by measuring the percentage of cells expressing cell-specific markers including, mucin 5AC (MUC5AC) as goblet cell marker, secretoglobin family 1A member (SCGB1A1) as club cell marker, and acetylated alpha-tubulin (ATUB) as ciliated cell marker[1] (**Fig. 1b-c**). Here, luminal cell boundaries were revealed by F-actin staining, allowing us to establish total and percentage of cells labeled with these markers (See Methods and **Supplementary Figs. S2 & S3**). Our results are summarized in **Fig. 1d** (for detailed breakdown see **Supplementary Tables S3 & S4**). Intriguingly, human airways presented with a continuously high ciliated cell proportion, or cilia coverage, of 88 ± 2% (SEM) across all analyzed BGs, whereas rat airways exhibited increasing cilia coverage along the airway tree, ranging from 44 ± 8% in trachea to 92 ± 1% in BG5. This contrasted with current literature which suggested a lower ciliation level of 30-50% in human trachea with increasing ciliation in higher BGs (**Supplementary Fig. S4**). On the other hand, our analysis of secretory cells matched trends reported in literature (**Supplementary Fig. S4**). In all examined human BGs, 10-20% of luminal cells were positive for either MUC5AC, SCGB1A1, or both. Within this secretory cell population, the proportion of MUC5AC+ SCGB1A1- (goblet), MUC5AC+ SCGB1A1- (club) and MUC5AC+ SCGB1A1+ (hybrid/transitionary) cells varied as a function of BG (**Fig. 1d**, inset). Goblet cells dominated the tracheobronchial region whereas club cells became most frequent in BG3 and higher. We also observed a significant proportion of MUC5AC+ SCGB1A1+ hybrid cells in all analyzed BGs, with mean values ranging between 15 and 30% of the labeled secretory population, similar to transcriptional and histological studies[22–24]. A comparable analysis was inconclusive for the rat secretory cells due to the overall low abundance of cells positive for MUC5AC and/or SCGB1A1 (<10%), which is consistent with literature[19]. However, rat airways are thought to contain a high abundance of so-called "serous" secretory cells[19] for which no protein markers have been reported, and therefore additional secretory cells could be present.

Human airways achieve higher clearance distance per ciliary beat cycle that rat airways

The differences found in ciliated cell coverage suggested functional changes in particle clearance, which we proceeded to explore by measuring live ciliary beat and fluorescent bead transport in the densely ciliated human airways (BG0 to BG6) compared to the sparsely ciliated rat airways (BG0 and BG1) (**Fig. 2a-b**). Ciliary beat frequency (CBF) recorded at room temperature was 2.9 ± 0.5 Hz human tissue and 4.7 ± 1.7 Hz in rat tissue. Associated particle clearance speed reached 11.6 ± 5.9 µm/s in humans and 5.6 ± 2.8 µm/s in rats. To compare particle clearance despite the differences in CBF, we derived the normalized "clearance speed per beat" (CPB) by dividing the average clearance speed by the average CBF for each field of view. CPB measures how far a particle is transported per ciliary beat cycle and has the units µm/beat. This analysis revealed a significantly higher normalized clearance speed in human tissue (4.2 ± 2.5 µm/beat) compared to rat tissue (1.2 ± 0.5 µm/beat) (**Fig. 2c**). We also investigated particle clearance directionality, defined as the net directional flow magnitude divided by total flow magnitude and ranges from 0 to 1, where a number near zero indicates stagnation or highly convoluted flow and a number near 1 indicates straight and unidirectional flow. Particle clearance directionality was higher in human tissues compared to rat tissues, indicating straighter and more aligned flow paths. However, since the surface of the *ex vivo* airways was often warped and distorted the particle trajectories, the data was noisy, and the difference did not reach significance. All measurements were completed in healthy and adult tissues that were washed, mucus-free and submerged in aqueous saline buffer,

suggesting that the differences in CPB and clearance directionality were due to species-specific properties of ciliary beat and organization[13] rather than defective[25] or immature ciliary beat[26], or altered mucus properties[27,28]. As intended by this comparison, coverage with ciliated cells was significantly higher in the human airways at BG0-6 (85.2 ± 2.8%) compared to rat airways at BG0-1 (55.4 ± 5.4%) (**Fig. 3a**). To capture additional differences, we measured key single cell and tissue-level ciliary beat properties (**Supplementary Fig. S5A**). On the cell-level, we measured average cilia length, ciliary beat amplitude, and the orientational order parameter of the ciliary beat angle (ciliary beat OP). The ciliary beat OP ranges from 0 to 1, where 0 means that the beat angles of ciliated cells in the field of view are randomly distributed, and 1 means that all beat angles are equal, resulting in spatial alignment of beat. At the tissue-level, we measured the distribution of ciliated cells in terms of the degree of patchiness, defined as the normalized spacing between ciliated areas[13], and in terms of crystalline order, defined as the relative variability of patchiness[13]. We found that patchiness and crystalline order were of similar magnitude between human and rat tissue, whereas cilia length was significantly higher in human compared to rat tissue (human: 7.1 ± 0.5 μm; rat: 5.1 ± 0.13μm). Ciliary beat OP and amplitude were also higher in human samples, but the difference did not reach significance (**Fig. 3a)**.

To understand how functional "output metrics" CPB and clearance directionality emerge from structural "input metrics," we developed a simple hydrodynamic model inspired by force singularity model of cilia[29–31] to simulate particle clearance due to cilia submerged in liquid, similar to our experimental measurement conditions (**Fig. 3b, Supplementary Figs. S5 & S6**). Here, we model each multiciliated cell as a single regularized Stokeslet that scales with cilia beat amplitude, points horizontally in the effective stroke direction, and is located at one cilia length above a no-slip wall that represents the stationary cell surface. The position of ciliated cells and the orientation of the corresponding Stokeslets are chosen so that the simulated epithelium conforms to the desired input metrics such as cilia coverage and ciliary beat OP, patchiness, and crystalline order parameter. Next, the resulting fluid velocity field and tracer particles trajectories were computed to derive CPB and clearance directionality as a function of cilia coverage. To validate the model, we confirmed that it correctly predicted the most dependable clearance measurements in human samples (i.e., from samples with minimal curvature), where a cilia coverage of 94% resulted in a CBP of 7.75 ± 1 μm/beat and a directionality value of 0.93 ± 0.2 (**Fig. 3c,** "human benchmark"). The model further predicted that CPB is linearly dependent on cilia coverage, while clearance directionality is a steeply rising function that exponentially converges to its maximum above a certain coverage fraction (**Fig. 3c**, red curves). We also computed these curves using the input parameters measured in rat airways. The predicted rat-specific curves (**Fig. 3c**, blue curves) fall below the human-specific curves because of the lower values in ciliary beat OP, amplitude, and cilia length in rats compared to humans (**Fig. 3a**), meaning that for identical cilia coverage, the maximal CBP and clearance directionality are lower in rats. Intriguingly, the experimentally measured values of CBP and clearance directionality again match the range predicted by the model (**Fig. 3c,** "rat BG0-1"), suggesting that despite its simplicity, our model captures key structure-function relationships.

Choice of culture medium drastically impacts cell type composition and clearance function

We next applied our structural and functional metrics of particle clearance to assess how human airway-like, aka "organotypic", differentiated cultures of primary human airway epithelial cells (pHAECs) were. We hypothesized that we could generate different luminal epithelial cell type compositions in the same cell donor by using a variety of cell culture differentiation media, as previously shown[32–34], thereby enabling us to compare the tissues grown in different media to native human *ex vivo* tissues both in terms of structural organization and clearance function. After expanding pHAECs in a common medium (Bronchial Epithelial Cell Medium (BEpiCM), Sciencell), we differentiated them for 28 days at air-liquid interface (ALI) in 5 different bronchial or small airway epithelial cell culture media using N=3-6 cell donors (**Supplementary Tables S1 & S2**) with n=3 insert cultures each. We used BD, a mixture of BEpiCM™ and DMEM[35]; mAir, a modified version of Airway Epithelial Cell Growth Medium (AECGM™, PromoCell)[33]; SAGM™ (Small Airway Epithelial Cell Growth Medium, PromoCell); PC (PneumaCult™-

ALI Medium, STEMCELL Technologies); or PC-S (PneumaCult™-ALI-S Medium, STEMCELL Technologies). Based on immunofluorescence (IF) staining, we found that cultures differed dramatically in their proportions of ciliated, club, goblet, and hybrid secretory cells depending on culture medium (**Fig. 4a**). in all donors, BD, mAir, and SAGM cultured tissues exhibited relatively low ciliation and contained a substantial proportion of unidentified luminal cells whereas PC and PC-S cultured tissues most closely resembled the average *ex vivo* composition measured in BG0-6 (**Fig. 4b**). Principal component analysis (PCA) of all measured metrics (**Supplementary Table S5**) revealed that ciliated and secretory cell proportions as well as the ratio between club and goblet cell proportions are key discriminatory metrics that organize the different *in vitro* conditions. Mapping the data onto these three dimensions showed that PC-generated cellular compositions were most like human *ex vivo* BG2-6 samples, whereas all other media conditions differed starkly from human *ex vivo* samples in one, or more, metrics (**Fig. 4c**).

Mirroring these compositional characteristics, only PC-cultured pHAECs achieved human *ex vivo*-like particle clearance function in terms of CPB (6.5 ± 2.3 µm/s) and directionality (0.74 ± 0.15), (**Fig. 5a**). In contrast, particle clearance in pHAECs cultured in other media conditions performed below the human *ex vivo* benchmarks and more closely resembled rat *ex vivo* clearance. To understand the mechanistic underpinnings, we assessed all ciliary input metrics. Cilia coverage, cilia length, beat amplitude, and patchiness varied the most in response to different differentiation media. Notably, BD and SAGM-cultured pHAECs had, on average, shorter cilia than human *ex vivo* samples (BD: 5.9 ± 1µm; SAGM: 5.2 ± 1.5µm; human: 7.13 ± 0.5µm), and only PC-cultured pHAECs reached human organotypic ciliary beat amplitudes (PC: 12.8 ± 1.4µm; human: 12.9 ± 0.9µm) (**Fig. 5b**). To assess the functional impact of these differences, we entered the ciliary input metrics of each medium condition into our computational model to predict CBP and particle clearance directionality as a function of cilia coverage (**Fig. 5c**). Overlaying the measured CBP and directionality values demonstrated a good fit with the model predictions overall, suggesting that our ciliary input metrics alone can be used to predict particle clearance function and explain its divergence from organotypic performance. The notable exception were PC-S cultured tissues, which performed well below the predicted curve, indicating that additional factors not assessed in this study, such as the beat waveform of individual cilia[26], may be sub-optimal.

Structural and functional maps of mucociliary clearance enable phenotypic benchmarking

In *in vitro* airway cultures, development of directional particle clearance depends on the hydrodynamic interaction of dense ciliation with a sufficiently viscous mucus layer; this interaction aligns ciliary beat during differentiation, leading to long-range clearance[36,37]. Mucus viscosity depends on the proportions and abundance of secretory cell types[27,38]; however, tools to assess this relationship remain limited, especially given the difficulty of measuring mucus rheology in miniscule *in vitro* samples[39]. We therefore evaluated whether the key variants in ciliated and secretory cell type composition (**Fig. 4c**) could be directly predictive of average clearance directionality in the human BG0-6 samples and the *in vitro* cultures. Indeed, a simple linear regression model resulted in a solid prediction of clearance directionality using as input the percentage of ciliated cells, percentage of secretory cells, and ratio of club to goblet cell proportions (**Fig. 6a**, R^2 =0.78). Using the percentage of ciliated cells as sole input, or removing it from the input, worsened the prediction (R^2 =0.63 and R^2 =0.53, respectively), showing that the combination of secretory and ciliated cell data was most predictive. Taken together, this analysis revealed that (1) structural ciliary metrics, especially ciliated cell coverage, are mechanistic predictors of particle clearance function; (2) the choice of cell culture medium greatly impacts ciliary metrics, especially ciliated cell coverage, and hence particle clearance function, and (3) luminal secretory and ciliated cell type composition may be a statistical predictor of particle clearance directionality.

Finally, to demonstrate the broader applicability of our analysis, we leveraged the structural cell-type composition map (**Fig. 4c**) and the functional CPB-against-cilia coverage map (**Fig. 5c**) to assess the mucociliary machinery in additional culture conditions and animal models, where the data was derived from literature or via proof-of-concept experiments (**Fig. 6b-c**). The systems we evaluated included

mature and developing mouse trachea, human airway epithelial cultures derived from induced pluripotent stem cells (iPSC), cultures subjected to asthma-like inflammatory conditions (interleukin-13 (IL-13) treated), and cultures differentiated under mechanical stimulation (Organ-on-Chip models). We found that iPSC-derived airway epithelial tissue differentiated in PC for 35 days at ALI (iALIs) as described earlier[40] exhibited suboptimal CPB given their cilia coverage, suggesting that ciliated cell function and organization was still immature in these tissues (**Fig. 6b**, purple hexagon). Secretory and ciliated cell type composition in iALIs (**Fig. 6b**, purple circle) resembled human BG0-6. The CBP of pHAECs differentiated in BD was also below the benchmark curve at day 14 of ALI when cultured in conventional static inserts (**Fig. 6b**, light green square) and approached the curve when cultured in continuously perfused Organ-on-Chip conditions (**Fig. 6b**, blue square). Further, after a prolonged culture time of 35 days, the insert ALI-cultures not only increased ciliation, but also reached the benchmark curve, indicating delayed maturation of ciliary beat (**Fig. 6b**, dark green square). Luminal cell type composition in both insert and chip conditions (**Fig. 6c**, light green and blue circles) reflected a lack of ciliation compared to the human benchmark of near 85%; however, the Organ-on-Chip cultures reached organotypic proportions of secretory cells[35]. The CBP of pHAECs cultured in Vertex ALI medium[41] fell below the benchmark curve at day 35 of ALI (**Fig. 6b**, black outlined star). Cultures treated with IL-13 for the final 14 days lost cilia coverage and, despite ciliary beat, generated almost no flow at all (CBP near zero). The cell type composition map reflects the high proportion of secretory cells expected from culture in Vertex ALI medium[41] (**Fig. 6c,** black outlined circle), and IL-13 treatment creates the expected sparsely ciliated, goblet-cell dominated Th2-like asthmatic phenotype induced by IL-13 treatment[42] (**Fig. 6c,** black solid circle). Ciliation and CBP in mouse trachea continue to increase after birth until, at approximately postnatal day (P) 15, they reach their mature performance at 40-45% ciliation[43] (**Fig. 6b**, light grey crosses and black cross, respectively). The nonlinear trajectory indicates that ciliary beat properties mature along-side with increases in ciliation. The mature performance resembles rat tracheobronchial data (**Fig. 6b**, light blue cross and model prediction) and hence it is possible that mouse and rat trachea share similar ciliary input metrics.

DISUSSION AND CONCLUSION

Our study reveals key differences in ciliation along the human and rat airway tree. We found that human airways are close to 90% ciliated from the large to the small airways, which contrasts to the gradual increase in ciliation starting from 45% in the trachea along the rat airway tree. A similar ciliation gradient reported in humans[19,44] likely stems from analyzing total epithelial tissue composition instead of luminal analysis. A preprint reporting luminal cilia coverage in the human small airways matches our estimate of 85%[45].

We developed a quantitative framework to predict the functional consequences of such differences in cilia properties on particle clearance. This framework establishes quantitative benchmarks of particle clearance as a function of cilia coverage, enabling the direct comparison between native human and engineered tissues, as well as animal models. The near 90% ciliation and associated clearance distance per beat of 8 µm/beat we found in the human airways does not support the idea that the ~40% cilia coverage (and associated CBP of 0.7 µm/beat) measured in mouse trachea is a conserved feature between species, as proposed[13]. The mouse airways also differ from human airways in many other aspects relevant to MCC, including near 100-fold smaller spatial dimensions, a different branching morphology, and the absence of mucus-producing goblet cells in healthy conditions[46], similar to the low proportions of secretory cells we found in the rat airways. In contrast, dogs and pigs are reported to have complete ciliary coverage in the large airways, similar to humans[47,48]. Together, this raises the question if MCC operates under different physical constraints in humans and other larger animals compared to rodents. Indeed, levels and size distributions of inhaled particle deposition vary greatly between humans and obligatory nose breathers such as rodents, and between different regions of the human airways[49]. In general, obligatory nose breathers such as rats and mice clear most particles in their nasal passages while in humans, most particles get absorbed in the large airways[50]. This might indicate different needs

for particle capture in the human large airways, such as greater mucus production coupled with higher ciliation to ensure clearance. In contrast, small particulate matter can reach the similarly sized rodent airways and human small airways where mucus, an otherwise effective particle trap, could create dangerous plugs, potentially necessitating a similar, mucus-free clearance strategy in both humans and rodents. Such implications remain speculative since our model does not capture the effects of mucus properties and hence future work should focus on adding mucus-cilia interactions to our quantitative understanding of particle clearance.

More generally, the two maps we developed, one based on ciliated and secretory cell composition (**Fig. 6c**), one representing particle clearance function (**Fig. 6b**), enable the quick comparison of different samples, such as pHAEC cultures, to a human organotypic benchmark. Although other studies have compared pHAEC differentiation in different media[51,52], they did not establish benchmarks representing native human airway epithelia. Our study is first to enable an evaluation of culture conditions in terms of their ability to generate organotypic structural and functional characteristics of MCC. Intriguingly, we demonstrated that secretory cell type abundance and composition may be a statistical indicator of clearance directionality, consistent with previous work showing the important role of mucus during differentiation for long-range clearance[36]. This relationship provides impetus for future work on mucus microrheology and models of cilia-mucus interactions. Our data also provide insight into the degree of variability that is to be expected in different model systems.

Due to the limited availability of healthy human lungs for scientific research, these data are based on only 12 human donors (**Supplementary Table S2**) and may not represent the full span of natural variability. Some of the analyzed human samples included lung cancer patients. The fact that high ciliation levels were nonetheless robustly high provides confidence that this is a key feature of the human airways. We also observed the expected trend of higher goblet cell to club cell ratios in BG0 and BG1, and a reversal of ratios in higher BGs. Therefore, the data presented here serves as a guide until additional studies refine the picture.

Taken together, our structure-function analysis of the mucociliary machinery along the human airway tree provides quantitative benchmarks and visualization tools to assess how human organotypic the mucociliary barrier of commonly used rodent and *in vitro* models are. The same analysis can also be used to probe the impact of maturation, treatments, and diseases on MCC. Our physics-based model enables the prediction of the impact of changes to cilia properties on particle clearance due to disease-mediated changes or damage, or due to repair or recovery processes, which could also help set expectations for the effectiveness of treatments that aim to restore MCC.

METHODS

Cell and tissue sources.
Source of rat airways. Rat lungs were harvested from freshly euthanized animals used for other research purposes that were performed according to approved animal study protocols. The animals investigated at USC were 3-8 months-old female Wistar-Kyoto rats (Charles River), and the animals investigated at Helmholtz/TUM were 8-week-old female Wistar rats (Charles River) (**Supplementary Table S1**).

Source of whole human lung and cells at USC. Human lung tissue from subjects with no prior history of chronic lung disease was obtained through the International Institute for the Advancement of Medicine (IIAM) with approval from the Institutional Review Board (IRB) of the University of Southern California (USC) (Protocol number: #HS-18-00273). Donor demographics are included in **Supplemental Table S1**. Human tracheobronchial epithelial cells (HTBECs) were isolated as previously described[53]. Briefly, proximal airways including the trachea, main stem bronchi and 2 further branching generations of the cartilaginous airways were dissected into 1-4 cm^2 sections and digested in of 0.1% Protease XIV (Sigma

#P5147) and 0.001% DNase (Sigma #DN25) (%w/v) in DMEM/F12 (ThermoFisher #11330032) overnight at 4°C. Using a scalpel, epithelial tissue was gently scraped, collected in DMEM/F12, and centrifuged at 400 x g for 5 minutes. After red blood cell lysis in ACK lysis buffer (ThermoFisher #A1049201), epithelial cells were single cell dissociated by incubation with Accutase (Innovative Cell Technologies #AT104) at 37°C for 30 minutes. Cells were then seeded at a density of 30K cells/cm^2 on PureCol (Advanced Biomatrix #5005) coated tissue culture dishes in airway epithelial growth media (Promocell #C-21160) and passaged at 80% confluence. At each passage cells were seeded at 5x10^3 cells/cm^2.

Source of human bronchial rings at LUMC. Bronchial rings were dissected from macroscopically normal lung tissue obtained from patients undergoing resection surgery for lung cancer at the Leiden University Medical Center, the Netherlands (**Supplementary Table S1**). Patients from which this lung tissue was derived were enrolled in the biobank via a no-objection system for coded anonymous further use of such tissue (www.coreon.org). However, since 01-09-2022, patients are enrolled in the biobank using written informed consent in accordance with local regulations from the LUMC biobank with approval by the institutional medical ethical committee (B20.042/Ab/ab and B20.042/Kb/kb). No clinical data from the patients from which the tissues were derived for this study are available.

Source of cells at TUM/Helmholtz. Cells were sourced from commercial suppliers (**Supplementary Table S1**).

Source of iPSC-derived cultures. See section on "Data for comparative CBP and cell type composition map."

Human primary airway epithelial cell culture. Human primary small airway epithelial cells (hSAECs) and tracheobronchial cells (hTBECs) were obtained from Lifeline Cell Technologies (USA) or via direct isolation from primary tissue (**Supplementary Table S1**). The first passage cells were expanded in collagen I coated T75 tissue culture flasks and dishes in standard bronchial epithelial cell medium (BEpiCM) (Sciencell (Sanbio), SCC3211-b) until ~90% confluency. Expanded small airway and bronchial/tracheal cells were seeded on collagen IV (300 µg/mL) coated 12-well 0.4 pore diameter PET Transwell membranes (Corning, 3460) at a density of 150K cells per insert (~135K cells/cm²). The cells from each donor were cultured in 1 nM EC23 (Tocris Bioscience) containing standard bronchial epithelial cell medium (BEpiCM) until confluent. Once the tissue was confluent, differentiation was induced by introducing air liquid interface (ALI) via removal of the apical medium (day 0 of ALI culture) and using one of five different differentiation medium in the basal compartment: 1. BD: bronchial epithelial base medium and Dulbecco's modified eagle medium BEpiCM:DMEM (50:50) with addition of supplements and 50 nM EC23[35]; 2. PC: PneumaCult ALI (STEMCELL Technologies); 3. PC-S: PneumaCult ALI-S (STEMCELL Technologies); 4. SAGM: Small Airway Epithelial Growth Medium (Promocell, C-21170) containing 50 nM EC23; and 5. mAir: a 1:1 mix of Dulbecco's modified eagle medium and Airway epithelial cell growth medium (AECGM, PromoCell, C-21160) with AECGM supplements and 50 nM EC23 (previously described in [33].) The apical surface was washed with phosphate-buffered saline (PBS, no Calcium and Magnesium) at 37 degrees twice a week to remove excess mucus. Cultures were differentiated until day 28 of ALI.

Live ciliary beat and particle clearance recordings.
Ex vivo samples. We freshly isolated airway epithelial tissue from respiratory tree branching generation (BG) 0 through BG6 from healthy transplant-rejected human whole lungs, and BG0 through BG5 from healthy rat whole lungs for live measurements. The human BG6 samples were at or below 2 mm in diameter (**Supplementary Fig. S1**) and therefore constituted the transition to small airway morphology as conventionally defined[54]. Samples were cut open along the airway tube to reveal the luminal epithelium, submerged in ice-cold HBSS buffer, mounted upside down in a glass bottom dish (ibidi), and gently flattened using a glass cover slip held down with silicone grease at the corners. Phase contrast

recording at high frame rates (100-200 fps) were performed at room temperature using an inverted Leica microscope equipped with a 40x (NA 0.8) objective and a PCO Edge 4.2 high speed camera (Excelitas Technologies), which was operated using the micromanager plugin (ImageJ). Cilia were live-stained with fluorescent-dye conjugated wheat germ agglutinin (ThermoFisher; 20 minute incubation in dilution of 1:200)[10] and 1-μm fluorescent tracer particles were added to the bath, such that live ciliary beat and particle clearance could be recorded in the same field of view for 10 seconds at 30 fps using epifluorescence imaging as previously described[35]. Two to four FOVs with visible CBF were recorded from each sample.

In vitro cultures. In vitro cultures were washed for 10 minutes with PBS and recorded at ALI using an inverted Zeiss microscope equipped with a 40x (NA 0.8) phase contrast objective and a temperature-controlled chamber that was preheated to 37°C. Movies were taken at 140 fps using an Orca Flash 4.0 camera (Hamamatsu). To reveal beat kinematics of thicker cultures, samples were mounted upside down and cilia were live-stained with fluorescent-dye conjugated tomato lectin (IVISense™ Tomato Lectin 680, Perkin Elmer) by incubating the sample in a 0.25 μM dilution in PBS for 20 minutes. After rinsing, ciliary beat kinematics were recorded at 30 fps using epifluorescence imaging. Clearance was recorded for 10 seconds as before[35] by adding 1-μm fluorescent tracer particles to the apical surface. Video recordings were made from 2 insert cultures per donor and condition, with at least 8 FOVs per sample.

Ciliary input metrics.
Cilia length in ex vivo samples. Hematoxylin & eosin (H&E)-stained sections of human bronchial rings and rat airway trachea were imaged using a Zeiss Axioscope 7 fluorescence microscope and a 40x oil DIC objective (NA 1.4). Cilia length data were measured manually using the freehand line tool in the image processing software Fiji ImageJ [55]. Only cilia with visible starting and end point were measured. For each rat donor, on average 15 FOVs were analyzed and on average 10 cilia were measured in each FOV. For each human donor, on average 4 FOVs were analyzed and on average 30 cilia were measured in each FOV.

Cilia length in in vitro samples. The cell layer was dissociated by incubating the cultures for 20 min in prewarmed Accutase (Invitrogen, 00-4555-56) in a conical tube. After 20 min warm culture medium was added at a ratio of 3:1 and the cells were centrifuged at 210× g for 7 min. The resulting pellet was resuspended in 500 μL 4% paraformaldehyde and 10 μL of this suspension was placed onto a glass bottom imaging dish (ibidi,81218-200) and covered with a glass coverslip. Cilia length was measured as above. For each donor, 30 FOVs were analyzed and on average 10 cilia were measured in each FOV.

Ciliary beat frequency (CBF). CBF was measured by applying Fourier spectral analysis to each cilia-associated pixel recorded in high-speed videos as previously described[17].

Ciliary beat order. We determined ciliary beat angle using manual tracing of beat direction from all ciliated cells in at least 3 FOVs. We derived the director-free ciliary beat order parameter (OP) from the angle distribution as follows: $OP = \sqrt{\langle \sin\theta \rangle^2 + \langle \cos\theta \rangle^2}$, where $\langle \rangle$ indicates the mean and θ indicates the measured angles.

Ciliary beat amplitude. We measured ciliary beat amplitude by manually tracing the span of the ciliary beat using kymographs of videorecordings[56] in at least 10 ciliated cells each in 3 FOVs.

Cilia coverage, cilia patchiness and crystalline order. These metrics were measured from images with IF-stained cilia. Images were thresholded and binarized to reveal the ciliation pattern, and ciliated cell patchiness and crystalline order were estimated as shown previously[13]. Briefly, a 2-point correlation function was used to measure the probability that two pixels at a certain distance from each other both have a binary intensity level of "1", i.e., are part of a ciliated cell. Running this analysis over each pixel in

the image and averaging the probabilities as a function of distance results in an oscillating function whose first local maximum reveals λ, the average spacing of two ciliated patches. Normalizing λ by dividing by the height of the ciliated carpet (ca. 10 μm) results in the non-dimensional cilia patchiness value. The crystalline order parameter (COP) describes the degree of variability of the patchiness between multiple FOVs and is derived from the average of λ and its standard deviation std(λ) across FOVs as follows: $COP = \frac{1-\sqrt{2}*std(\lambda)}{mean(\lambda)}$. Cilia coverage, defined here as percentage of luminal cells that are ciliated, was determined as part of the cell type composition analysis discussed in the associated methods section.

Particle clearance output metrics. The displacement and trajectories of fluorescent tracers driven by ciliary beat was automatically measured using the open source ImageJ Trackmate plugin[57]. From these data, two metrics were calculated.

Particle clearance directionality. Particle clearance directionality was defined as the Euclidian distance traveled by a particle divided by total trajectory length, or in the Eulerian framework, as the magnitude of the average flow vector divided by the average magnitude of all flow vectors, i.e., clearance directionality = $|\langle v \rangle|/\langle|v|\rangle$, where $\langle \rangle$ indicates the mean and $||$ indicates the magnitude of each vector *v* in the vector field described by the particle trajectories.

Clearance distance per beat. Clearance per beat (CPB) was defined as the mean speed of particle clearance (in units of μm per second) divided by the ciliary beat frequency (beats per second), resulting in units of μm per beat. This is a measure of the efficacy of each ciliary beat cycle in driving particle clearance. When both speed and CBF data were available for the same FOV, CPB was computed directly from the ratio. When speed and CBF data were recorded separately, their mean values over multiple fields of views were used to compute one single value of CPB from their ratios.

In ex vivo samples, the surface topography was often distorted due to elastic recoil after cutting the cartilage rings, leading to contorted tracer trajectories and variable distance between tracer particle and cilia, which impacts apparent clearance speeds (**Supplementary Fig. S7**). To establish robust benchmarks and to validate the physics-based model, we used the clearance measurements from samples that we trusted the most, i.e., measurements from entirely flat airway sections where the particles were visibly touching the cilia.

IF staining and imaging.
Human and rat airway sections. Isolated airway tube sections were fixed using a 4% paraformaldehyde (PFA) solution for 3 to 24h depending on tissue thickness, washed with PBS, and stored in PBS at 4 °C until staining. Prior to staining, the diameters of the sections were measured using a ruler. For large airway rings, nearly level sections were dissected at the region of the cartilage to minimize warping of the epithelium after severing the muscle. Small airway samples without cartilage were cut along the tube and flattened out for imaging. Samples were placed into a 96-well plate for staining.

*Human airway epithelial cell culture*s. After differentiation at ALI, the pHAEC and iPSC-derived cultures were fixed using incubation with 4% PFA solution for 30 min at RT, then washed again three times with PBS and stored in PBS at 4 °C until staining.

IF staining. Samples were blocked and permeabilized using 0.25% (v/v) Triton-X 100 in PBS with 3% BSA for 60 min at RT, then incubated overnight at 4 °C with primary antibodies against Mucin5AC and Uteroglobin/ SCGB1A1 diluted in the Triton/BSA buffer (**Supplementary Table S6**). The samples were rinsed three times for 5 min with PBS before incubation with secondary antibodies diluted in Triton/BSA buffer for 1 h at 37 °C, followed by a triple 5 min wash with PBS. Then, the samples were incubated with directly conjugated anti-alpha-tubulin primary antibody and F-actin stain phalloidin 555 (Invitrogen, A30106) or phalloidin 405 (Invitrogen, A30104) in Triton/BSA buffer for 1 hour at 37 °C, followed by a

triple 5 min wash with PBS. The samples were stored at 4 °C until mounting. For mounting, *ex vivo* samples were placed into glass-bottom imaging dishes (ibidi, 81218-200) and covered with SlowFade™ Glass Antifade Mountant (Invitrogen, S36917). A round coverslip lined with silicone grease was used to push down and flatten the sections. The *in vitro* samples were mounted by removing the cell culture membrane from the insert using a scalpel and placing the membranes onto glass slides with the cells facing upwards, followed by the addition of ProLong™ Diamond Antifade Mountant (Invitrogen, P36965) and a round number 1.5 glass coverslip.

IF imaging. Human bronchial ring sections were imaged using a Leica DMi8 microscope equipped with an Andor Dragonfly 200 spinning disk confocal and a 40× water objective (NA 0.80). From every stained ring section, 3 to 8 FOVs with a size of 2048 x 2048 pixels were recorded. Rat samples, other human airway sections, and *in vitro* cultures were imaged using a Leica confocal scanning microscope or a Zeiss Axioscope 7 fluorescence microscope equipped with a 40x oil DIC objective (NA 1.4). Six FOVs with a size of 2048 x 2048 pixels were recorded per sample.

Cell type composition analysis. We employed semi-automated image analysis to quantify luminal cell type composition from IF images (**Supplementary Fig. S2**). Using ImageJ Fiji[55], raw image data was converted to 16 or 8-bit tiff images using maximum projection for stacks. As needed, images were cropped to remove edge artifacts and the subtract background function was applied with a rolling ball radius of 1000 pixels. The Fiji plugin Advanced Trainable Weka Segmentation with all default and the Laplacian, Derivatives and Structure training features[58] was used to segment cell outlines from the F-actin mesh. Cell marker channels (MUC5AC, SCGB1A1, and acetylated alpha-tubulin) were filtered and optimized in contrast. After these preprocessing steps, cell type composition analysis was performed by overlaying the cell marker channels with the cellular outlines using CellProfiler™[59], providing total cell number and proportions of acetylated α-tubulin positive, MUC5AC positive, SCGB1A1 positive, and MUC5AC and SCGB1A1 double-positive cells.

Airway histology and imaging.
Rat trachea. Tracheas were obtained from wildtype Wistar rats and fixed in 2% PFA at 4°C overnight on an orbital shaker. Tracheas were washed 4 times in PBS for 10 minutes at room temperature with constant shaking and were embedded into paraffin wax in a lateral (dorso-ventral) orientation. Traditional H&E staining was performed and microscopical images at 400x magnification were taken of all sections, with at least 6 FOVs per trachea.
Human bronchial rings. Bronchial rings were obtained from tumor-free resected lung tissue at the Leiden University Medical Center. The rings were fixed using 4% PFA solution for 24 hours after which the rings were transferred to PBS and stored at 4°C until paraffin embedding at the Department of Pathology at the Leiden University Medical Center. Bronchial ring sections were deparaffinized in xylene and dehydrated in an ethanol gradient. Traditional H&E staining was performed and microscopical images at 400x magnification were taken of all sections, with at least 3 FOVs per sample.

Statistical analysis. For each metric, the average of the entire FOV was determined, and by averaging this value across all FOVs taken from all samples of the same condition, a single value for each metric was established for each donor and condition. See **Supplementary Table S2** for donor numbers for each condition and measurement. Where noted in the figures, statistical analysis of differences between the median values was performed using the non-parametric Kruskal-Wallis test.

Linear regression model. The model was created in MATLAB using the regression learner application.

Data for comparative CBP and cell type composition map

Mouse tracheal CPB. CPB in developing mouse trachea between postnatal days (P) 0 and 29 (grey crosses in Fig.6b) in were derived from Toskala *et al*[60]. CPB in mature mouse trachea at P15 (black cross in Fig.6b) was derived from Ramirez-San Juan *et al*[13].

Airway-on-Chip and insert cultures of pHAEC in BD. CPB and cell type composition were derived from previous studies[35].

IL-13 treatment of pHAEC cultures in Vertex ALI medium. pHAEC were differentiated in Vertex ALI medium[41] for 21 days at ALI. A chronic airway inflammatory phenotype was induced by treatment with 100 ng/mL of IL-13 (Invitrogen, A42525) for 14 days. Analysis of CBP and cell type composition was conducted at day 35 ALI as described above.

Generation and analysis of iPSC-derived respiratory cultures (iALI cultures). Differentiation of human iPSCs (hiPSCs) towards respiratory epithelium was performed as described previously[40]. Briefly, hiPSCs were differentiated to definitive endoderm by using the STEMdiff™ Definitive Endoderm Kit (STEMCELL Tech., Vancouver, BC, Canada). Subsequently, cells were dissociated and replated for anterior foregut induction by supplementing basis medium with 10 µM SB431542 (provided by the Institute of Organic Chemistry, Leibniz University, Hannover, Germany), and 3 µM Dorsomorphin (Sigma Aldrich, Saint Louis, MO, USA) for 24 hours, followed by supplementation with 2 µM IWP2 (Tocris, Bristol, UK) and 10 µM SB431542 for another 24 h. For lung lineage specification, basis medium was supplemented with 10 ng/mL BMP4 (R&D Systems, Minneapolis, MN, USA), 10 ng/mL FGF10 (R&D Systems, Minneapolis, MN, USA), and 3 µM Chir99021 (provided by the Institute of Organic Chemistry, Leibniz University, Hannover, Germany) until day 14 of differentiation. NKX2.1 positive lung progenitor cells were enriched by sorting for the cell surface marker carboxypeptidase M (CPM) (FUJIFILM Wako, Cat# 014-27501). To mature lung progenitor cells to ciliated respiratory epithelium, enriched cultures were seeded onto transwells (Greiner Bio-One, Frickenhausen, Germany) and expanded in small airway epithelial cell growth medium (SAECGM; PromoCell, Heidelberg, Germany) supplemented with 1% penicillin/streptomycin (Gibco, Billings, MT, USA), 1 µM A83-01 (Tocris, Bristol, UK), 0.2 µM DMH-1 (Tocris, Bristol, UK) and 5 µM Y-27632 (Tocris, Bristol, UK) for four days. Afterwards, medium was switched to PneumaCult™-ALI medium (STEMCELLTech., Vancouver, BC, Canada) and cells were differentiated in air-liquid interface conditions for 28 days before analysis. Analysis of CBP and cell type composition was conducted as described above for pHAECs.

Physics-based model.
Cell-level ciliary input parameters. We model the averaged forces generated by all cilia of a multiciliated cell as a single force monopole, located at one cilia length above a no-slip cell surface at z=0, in a semi-infinite domain, based on custom MATLAB (Mathworks) implementation of the regularized Stokeslet algorithm[61]. The regularized Stokeslet's strength is proportional to ciliary beat amplitude, with its direction corresponding to power stroke direction (**Supplementary Fig. S5A**).
While this approach cannot resolve the flow and coordination of individual cilia as in single-cilia models[29,62–65], it is straightforward to implement, suitable for large number of ciliated cells, and directly takes into account of the wall-screening effects due to finite cilia length comparing to the slip-boundary-velocity approach[13]. We did not consider the effects of double confinement or mucus film geometry discussed in Ramirez-San Juan *et al.* [13] because (i) we intend to compare tracer particle motions recorded at the cilia tip and sufficiently far from other confinement boundaries such as coverslip and air-liquid interface; (ii) experimentally, we chose appropriately-sized field-of-views such that no recirculation effects are observable; (iii) all functional measurements were done in washed samples without the presence of mucus.

Tissue-level ciliary input parameters. We derive the ciliated cell distribution based on a cilia coverage percentage and a crystalline order parameter as defined previously[13], where the order parameter relies

on the distribution of wavelength λ between each ciliated patch (**Supplementary Fig. S5A**). Here the mean and standard deviation of λ is determined based on structural measurements. Then ciliated patches are generated based on Gaussian displacement of cells that follow regular crystalline patterns, similar to the procedure reported in Ramirez-San Juan *et al* [13]. Each ciliated cell assumes a beat direction angle θ sampled from a Von Mises distribution, where its mean is set to be 0 (beating towards x-axis) and its second moment, or the orientation order parameter, is determined based on the measured cilia beat order. In the **Supplementary Methods**, we provide an exact description of how both cilia- and tissue-level parameters are implemented *in silico.*

Model output. The model uses a rectangular grid of 51 x 51 cells, doubly periodic in both x- and y-axis, where x-axis is defined as the clearance direction. Every cell is assumed to have a diameter of 10 μm, with its center slightly perturbed away from the exact grid points in Monte-Carlo simulations; for visual reference, cell boundaries are drawn based on the Voronoi diagram of the perturbed cell center points (**Supplementary Fig. S5B**). We implement the periodic boundary conditions by truncating hydrodynamic interactions further than one periodic image away (>250 μm) from any given point of interest. This introduces only a small error in the flow velocity because the no-slip surface at z = 0 causes a quadratic decay of hydrodynamic interactions. We derive ciliary flow characteristics from the trajectories of simulated tracer particles injected near cilia tip. Tracers are subject to both cilia-driven flow and thermal fluctuations. Since we do not vary particle size or fluid viscosity (mucus is removed in experiments), we fix the particle diffusivity to be D= 10^{-1} μm^2/s for micrometer-sized particles in water of viscosity μ = 10^{-3} Pa s. Time evolution of 500 initially uniformly distributed particles are computed for 500 beat periods, following the Langevin equation dr/dt = v_c(r) + (2D)$^{0.5}$η(t), where r is the particle position, v_c(r) the cilia-driven flow, and η(t) a standard Wiener process (white noise). Equations are numerically integrated with a Euler-Maruyama scheme, using periodic boundaries in both x- and y-directions. The main quantitative output of our simulation is the clearance per beat (CPB) and clearance directionality (**Supplementary Fig. S5A**).

Example flow pattern. To illustrate how tissue-level parameters affect our model output, we present example case studies (**Supplementary Fig. S5B**). The crystalline order parameter changes how ciliated cells are distributed; however, it does not strongly impact the characteristics of the tracer trajectories. Lowering cilia coverage or orientation order parameters reduces the clearance distance and directionality. In **Supplementary Fig. S6**, we present quantitative results of CPB and clearance directionality change with (1) cilia length, (2) cilia beat amplitude, (3) cilia beat order and (4) patch heterogeneity.

DATA AVAILABILITY

All relevant data supporting the key findings of this study are available in the article and its Supplementary information files or from the corresponding authors upon reasonable request. Raw image data will be made accessible at Figshare in the future.

CODE AVAILABILITY

The MATLAB implementation of the physics-based model will be made accessible in the future.

REFERENCES

1.   Whitsett, J. A. Airway Epithelial Differentiation and Mucociliary Clearance. *Annals ATS* **15**, S143–S148 (2018).

2. Wanner, A., Salathé, M. & O'Riordan, T. G. Mucociliary clearance in the airways. *Am J Respir Crit Care Med* **154**, 1868–1902 (1996).

3. Munkholm, M. & Mortensen, J. Mucociliary clearance: pathophysiological aspects. *Clin Physiol Funct Imaging* **34**, 171–177 (2014).

4. Nawroth, J. C., van der Does, A. M., Ryan (Firth), A. & Kanso, E. Multiscale mechanics of mucociliary clearance in the lung. *Philosophical Transactions of the Royal Society B: Biological Sciences* **375**, 20190160 (2020).

5. Satir, P. & Sleigh, M. A. The physiology of cilia and mucociliary interactions. *Annual review of physiology* **52**, 137–155 (1990).

6. Button, B. *et al.* A periciliary brush promotes the lung health by separating the mucus layer from airway epithelia. *Science* **337**, 937–941 (2012).

7. Davis, J. D. & Wypych, T. P. Cellular and functional heterogeneity of the airway epithelium. *Mucosal Immunol* **14**, 978–990 (2021).

8. Randell, S. H. & Boucher, R. C. Effective mucus clearance is essential for respiratory health. *Am. J. Respir. Cell Mol. Biol.* **35**, 20–28 (2006).

9. King, M. Experimental models for studying mucociliary clearance. *European Respiratory Journal* **11**, 222–228 (1998).

10. Nakamura, R. *et al.* A novel method for live imaging of human airway cilia using wheat germ agglutinin. *Sci Rep* **10**, 14417 (2020).

11. Schiller, H. B. *et al.* The Human Lung Cell Atlas: A High-Resolution Reference Map of the Human Lung in Health and Disease. *Am J Respir Cell Mol Biol* **61**, 31–41 (2019).

12. Liu, Y., Beyer, A. & Aebersold, R. On the Dependency of Cellular Protein Levels on mRNA Abundance. *Cell* **165**, 535–550 (2016).

13. Ramirez-San Juan, G. R. *et al.* Multi-scale spatial heterogeneity enhances particle clearance in airway ciliary arrays. *Nat. Phys.* **16**, 958–964 (2020).

14. Raidt, J. *et al.* Ciliary beat pattern and frequency in genetic variants of primary ciliary dyskinesia. *European Respiratory Journal* **44**, 1579–1588 (2014).

15. Heijink, I. H. *et al.* Epithelial cell dysfunction, a major driver of asthma development. *Allergy* **75**, 1898–1913 (2020).

16. Benam, K. H. *et al.* Small airway-on-a-chip enables analysis of human lung inflammation and drug responses in vitro. *Nature Methods* **13**, 151–157 (2016).

17. Benam, K. H. *et al.* Matched-Comparative Modeling of Normal and Diseased Human Airway Responses Using a Microengineered Breathing Lung Chip. *Cell Systems* **3**, 456-466.e4 (2016).

18. Sachs, N. *et al.* Long-term expanding human airway organoids for disease modeling. *EMBO J* **38**, (2019).

19. Mercer, R. R., Russell, M. L., Roggli, V. L. & Crapo, J. D. Cell number and distribution in human and rat airways. *Am J Respir Cell Mol Biol* **10**, 613–624 (1994).

20. Yang, J. *et al.* Smoking-Dependent Distal-to-Proximal Repatterning of the Adult Human Small Airway Epithelium. *Am J Respir Crit Care Med* **196**, 340–352 (2017).

21. Nawroth, J. C. *et al.* Motile cilia create fluid-mechanical microhabitats for the active recruitment of the host microbiome. *PNAS* **114**, 9510–9516 (2017).

22. Okuda, K. *et al.* Localization of Secretory Mucins MUC5AC and MUC5B in Normal/Healthy Human Airways. *Am. J. Respir. Crit. Care Med.* **199**, 715–727 (2019).

23. Deprez, M. *et al.* A Single-Cell Atlas of the Human Healthy Airways. *Am J Respir Crit Care Med* **202**, 1636–1645 (2020).

24. Okuda, K. *et al.* Secretory Cells Dominate Airway CFTR Expression and Function in Human Airway Superficial Epithelia. *Am J Respir Crit Care Med* **203**, 1275–1289 (2021).

25. Chilvers, M. A., Rutman, A. & O'Callaghan, C. Ciliary beat pattern is associated with specific ultrastructural defects in primary ciliary dyskinesia. *J. Allergy Clin. Immunol.* **112**, 518–524 (2003).

26. Oltean, A., Schaffer, A. J., Bayly, P. V. & Brody, S. L. Quantifying Ciliary Dynamics during Assembly Reveals Stepwise Waveform Maturation in Airway Cells. *Am J Respir Cell Mol Biol* **59**, 511–522 (2018).

27. Song, D. *et al.* MUC5B mobilizes and MUC5AC spatially aligns mucociliary transport on human airway epithelium. *Science Advances* **8**, eabq5049 (2022).

28. Bonser, L. R., Zlock, L., Finkbeiner, W. & Erle, D. J. Epithelial tethering of MUC5AC-rich mucus impairs mucociliary transport in asthma. *J Clin Invest* **126**, 2367–2371 (2016).

29. Kanale, A. V., Ling, F., Guo, H., Fürthauer, S. & Kanso, E. Spontaneous phase coordination and fluid pumping in model ciliary carpets. *Proceedings of the National Academy of Sciences* **119**, e2214413119 (2022).

30. Smith, D. J., Gaffney, E. A. & Blake, J. R. Discrete cilia modelling with singularity distributions: application to the embryonic node and the airway surface liquid. *Bull Math Biol* **69**, 1477–1510 (2007).

31. Blake, J. R. & Otto, S. R. Ciliary propulsion, chaotic filtration and a 'blinking' stokeslet. *J Eng Math* **30**, 151–168 (1996).

32. Saint-Criq, V. *et al.* Choice of Differentiation Media Significantly Impacts Cell Lineage and Response to CFTR Modulators in Fully Differentiated Primary Cultures of Cystic Fibrosis Human Airway Epithelial Cells. *Cells* **9**, 2137 (2020).

33. Luengen, A. E. *et al.* Choosing the Right Differentiation Medium to Develop Mucociliary Phenotype of Primary Nasal Epithelial Cells In Vitro. *Scientific Reports* **10**, 6963 (2020).

34. Bukowy-Bieryłło, Z. Long-term differentiating primary human airway epithelial cell cultures: how far are we? *Cell Communication and Signaling* **19**, 63 (2021).

35. Nawroth, J. C. *et al.* Breathing on chip: Dynamic flow and stretch accelerate mucociliary maturation of airway epithelium in vitro. *Materials Today Bio* 100713 (2023) doi:10.1016/j.mtbio.2023.100713.

36. Loiseau, E. *et al.* Active mucus–cilia hydrodynamic coupling drives self-organization of human bronchial epithelium. *Nat. Phys.* **16**, 1158–1164 (2020).

37. Gsell, S., Loiseau, E., D'Ortona, U., Viallat, A. & Favier, J. Hydrodynamic model of directional ciliary-beat organization in human airways. *Sci Rep* **10**, 8405 (2020).

38. Bonser, L. R. & Erle, D. J. Airway Mucus and Asthma: The Role of MUC5AC and MUC5B. *J Clin Med* **6**, 112 (2017).

39. Atanasova, K. R. & Reznikov, L. R. Strategies for measuring airway mucus and mucins. *Respir Res* **20**, (2019).

40. von Schledorn, L. *et al.* Primary Ciliary Dyskinesia Patient-Specific hiPSC-Derived Airway Epithelium in Air-Liquid Interface Culture Recapitulates Disease Specific Phenotypes In Vitro. *Cells* **12**, 1467 (2023).

41. Neuberger, T., Burton, B., Clark, H. & Van Goor, F. Use of primary cultures of human bronchial epithelial cells isolated from cystic fibrosis patients for the pre-clinical testing of CFTR modulators. *Methods Mol Biol* **741**, 39–54 (2011).

42. Atherton, H. C., Jones, G. & Danahay, H. IL-13-induced changes in the goblet cell density of human bronchial epithelial cell cultures: MAP kinase and phosphatidylinositol 3-kinase regulation. *American Journal of Physiology-Lung Cellular and Molecular Physiology* **285**, L730–L739 (2003).

43. Francis, R. J. B. *et al.* Initiation and maturation of cilia-generated flow in newborn and postnatal mouse airway. *American Journal of Physiology-Lung Cellular and Molecular Physiology* **296**, L1067–L1075 (2009).

44. Tilley, A. E., Walters, M. S., Shaykhiev, R. & Crystal, R. G. Cilia dysfunction in lung disease. *Annu. Rev. Physiol.* **77**, 379–406 (2015).

45. Dvornikov, D. *et al.* Quantitative imaging reveals PI3Kδ inhibition reduces rhinovirus-induced damage of small airway epithelia in ex vivo cultured human precision cut lung slices from COPD patients. 2022.03.01.482451 Preprint at https://doi.org/10.1101/2022.03.01.482451 (2022).

46. Danopoulos, S., Shiosaki, J. & Al Alam, D. FGF Signaling in Lung Development and Disease: Human Versus Mouse. *Frontiers in Genetics* **10**, (2019).

47. Gan, Y. *et al.* Establishment of a model of Mycoplasma hyopneumoniae infection using Bama miniature pigs. *Food Production, Processing and Nutrition* **2**, 19 (2020).

48. Wright, N. G., Brown, R. M. H., Mccandlish, I. A. P., Thompson, H. & Cornwell, H. J. C. Patterns of cilia formation in the lower respiratory tract of the dog: a scanning electron microscopic study. *Research in Veterinary Science* **34**, 340–346 (1983).

49. Wolff, R. K. Perspectives on Lung Dose and Inhaled Biomolecules. *Toxicol Pathol* **49**, 378–385 (2021).

50. Brown, J. S. Chapter 27 - Deposition of Particles. in *Comparative Biology of the Normal Lung (Second Edition)* (ed. Parent, R. A.) 513–536 (Academic Press, 2015). doi:10.1016/B978-0-12-404577-4.00027-8.

51. Leung, C., Wadsworth, S. J., Yang, S. J. & Dorscheid, D. R. Structural and functional variations in human bronchial epithelial cells cultured in air-liquid interface using different growth media. *American Journal of Physiology-Lung Cellular and Molecular Physiology* **318**, L1063–L1073 (2020).

52. Awatade, N. T. *et al.* Comparison of commercially available differentiation media on cell morphology, function, and anti-viral responses in conditionally reprogrammed human bronchial epithelial cells. *Sci Rep* **13**, 11200 (2023).

53. Fulcher, M. L., Gabriel, S., Burns, K. A., Yankaskas, J. R. & Randell, S. H. Well-differentiated human airway epithelial cell cultures. *Methods Mol Med* **107**, 183–206 (2005).

54. Hogg, J. C. *et al.* The nature of small-airway obstruction in chronic obstructive pulmonary disease. *N Engl J Med* **350**, 2645–2653 (2004).

55. Schindelin, J. *et al.* Fiji: an open-source platform for biological-image analysis. *Nat Meth* **9**, 676–682 (2012).

56. Yasuda, M. *et al.* Intracellular Cl- Regulation of Ciliary Beating in Ciliated Human Nasal Epithelial Cells: Frequency and Distance of Ciliary Beating Observed by High-Speed Video Microscopy. *Int J Mol Sci* **21**, 4052 (2020).

57. Tinevez, J.-Y. *et al.* TrackMate: An open and extensible platform for single-particle tracking. *Methods* **115**, 80–90 (2017).

58. Arganda-Carreras, I. *et al.* Trainable Weka Segmentation: a machine learning tool for microscopy pixel classification. *Bioinformatics* **33**, 2424–2426 (2017).

59. McQuin, C. *et al.* CellProfiler 3.0: Next-generation image processing for biology. *PLoS Biol* **16**, (2018).

60. Toskala, E., Smiley-Jewell, S. M., Wong, V. J., King, D. & Plopper, C. G. The temporal and spatial distribution of ciliogenesis in the tracheobronchial airways of mice. *Am J Physiol Lung Cell Mol Physiol* **289**, L454–L459 (2005).

61. Ainley, J., Durkin, S., Embid, R., Boindala, P. & Cortez, R. The method of images for regularized Stokeslets. *Journal of Computational Physics* **227**, 4600–4616 (2008).

62. Elgeti, J. & Gompper, G. Emergence of metachronal waves in cilia arrays. *Proceedings of the National Academy of Sciences* **110**, 4470–4475 (2013).

63. Ding, Y., Nawroth, J., McFall-Ngai, M. & Kanso, E. Mixing and transport by ciliary carpets: a numerical study. *Journal of Fluid Mechanics* **743**, 124–140 (2014).

64. Vilfan, A. & Jülicher, F. Hydrodynamic flow patterns and synchronization of beating cilia. *Phys. Rev. Lett.* **96**, 058102 (2006).

65. Uchida, N. & Golestanian, R. Generic conditions for hydrodynamic synchronization. *Phys. Rev. Lett.* **106**, 058104 (2011).
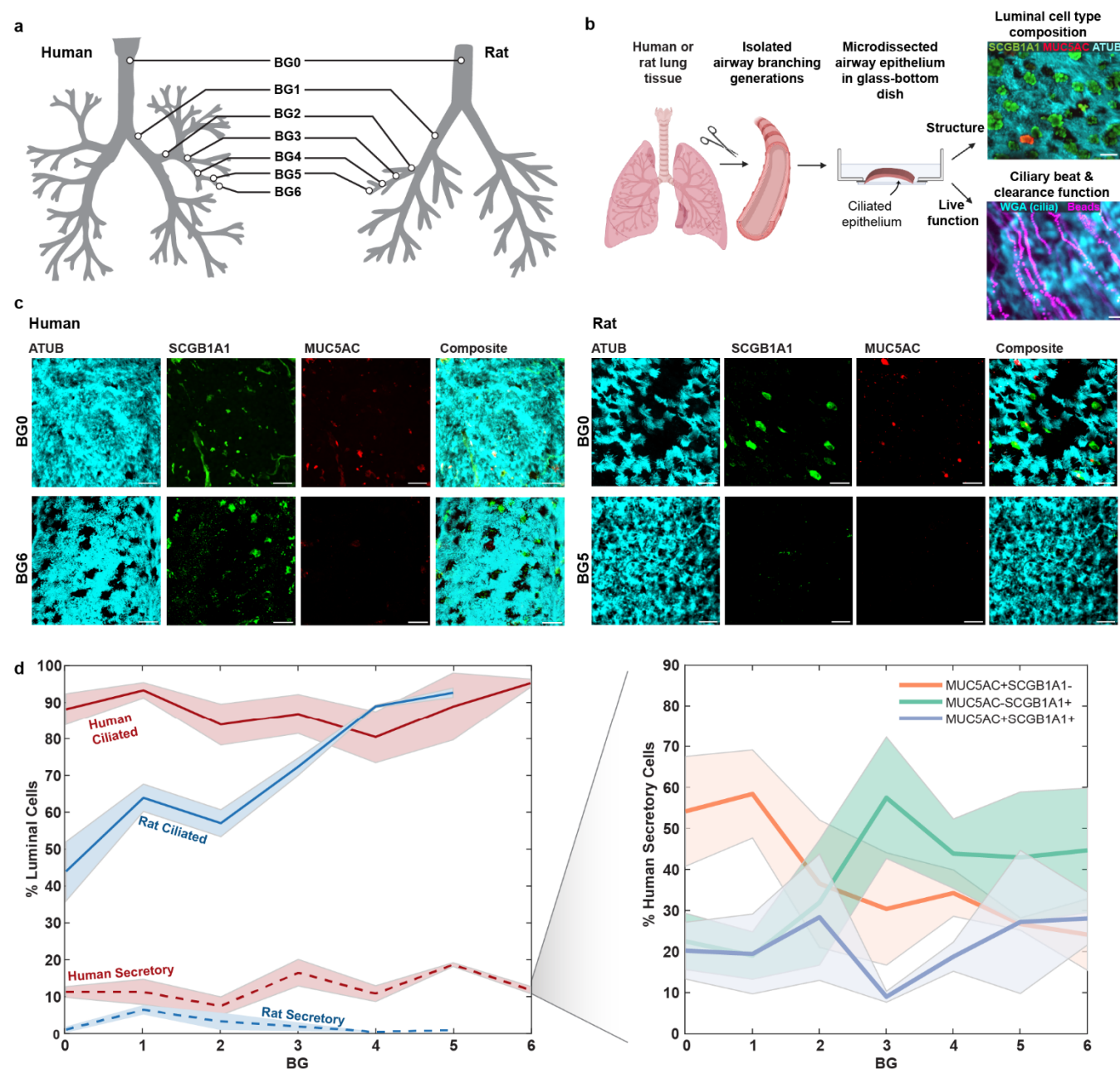
ACKNOWLEDGEMENTS

ETHICS DECLARATIONS

The authors declare no competing interests.

FIGURES

Figure 1: Luminal epithelial cell type composition along the human and rat airway tree. a, Airway branching generations in human and rat investigated in this study. b, Workflow for imaging luminal epithelial cell type composition and ciliary beat and clearance function in airway samples. c Representative IF staining of cilia (ATUB, cyan) and secretory cells (SCGB1A1, green; MUC5AC, red) in human and rat airway epithelium in BG0 (trachea) and BG5/6. Scale bar: 20 μm. D, Quantification of luminal cell proportions labeled with ATUB (ciliated cells) or with MUC5AC and/or SCGB1A1 (secretory cells) as a function of airway branching generation in human and rat airway epithelium. Inset: Percentage of human secretory cell population positive for only MUC5AC (orange), only for SCGB1A1 (green), or for both (purple) as a function of branching generation. Solid line: mean, shaded region: SEM.
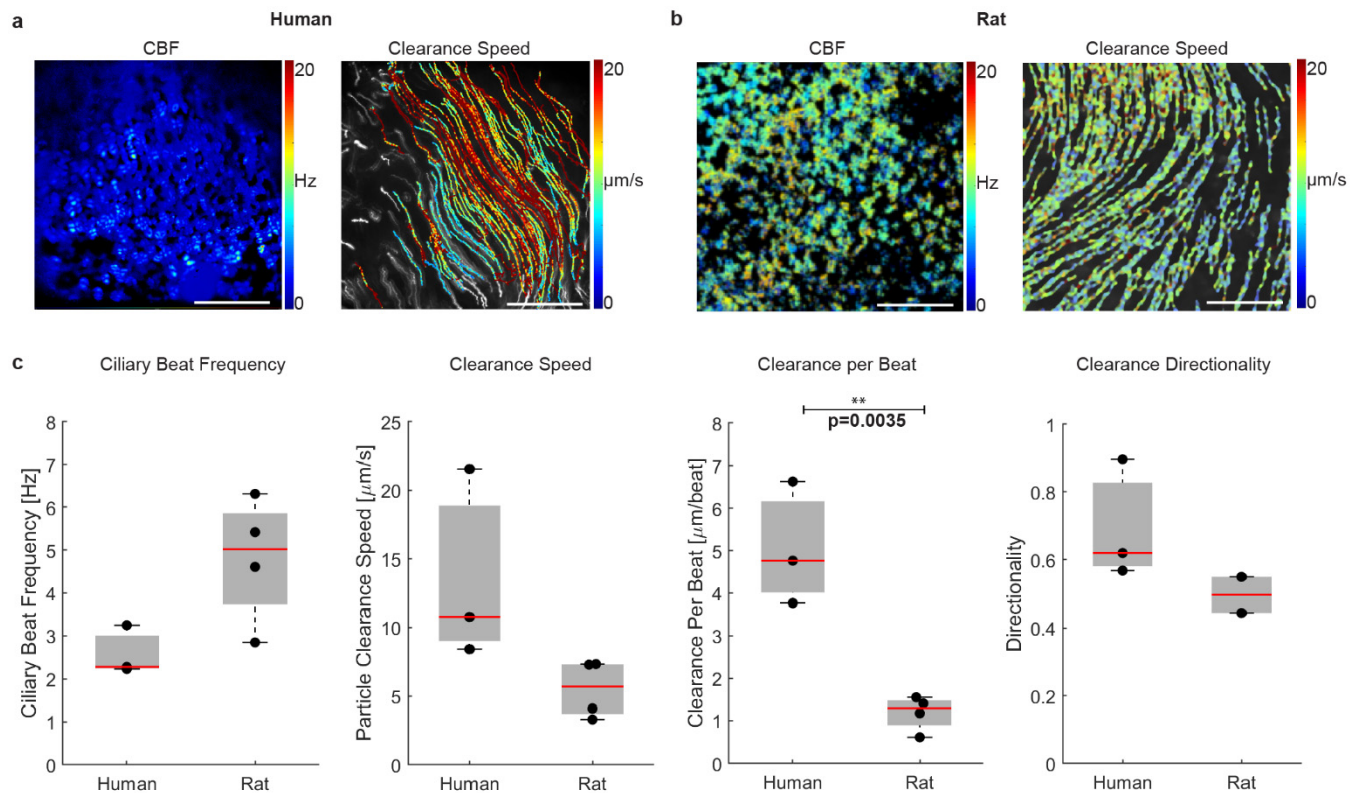
Figure 2: Ciliary beat and particle clearance function in human and rat airway epithelium. a, Representative measurement of ciliary beat frequency (CBF) and associated particle clearance trajectories in a human airway epithelial sample (BG2) compared to a rat airway epithelial sample (BG1). b, Quantification of average CBF and particle clearance speed in human and rat airways. c, Average clearance distance per beat (clearance speed divided by CBF) and clearance directionality in in human and rat airways. d, Solid dots are mean values per donor across multiple BGs; red line is median of distribution; significance was assessed with Kruskal–Wallis test.
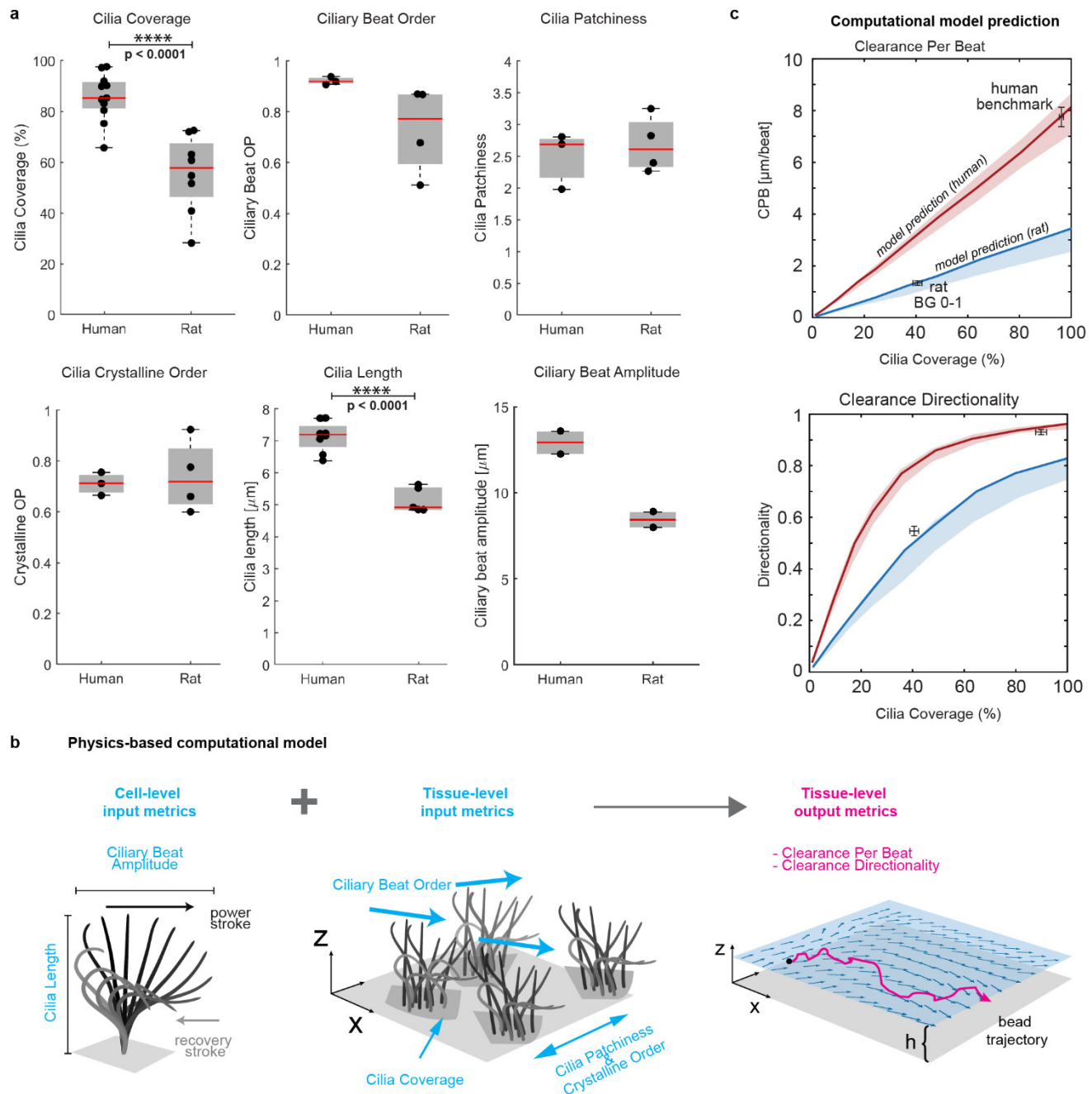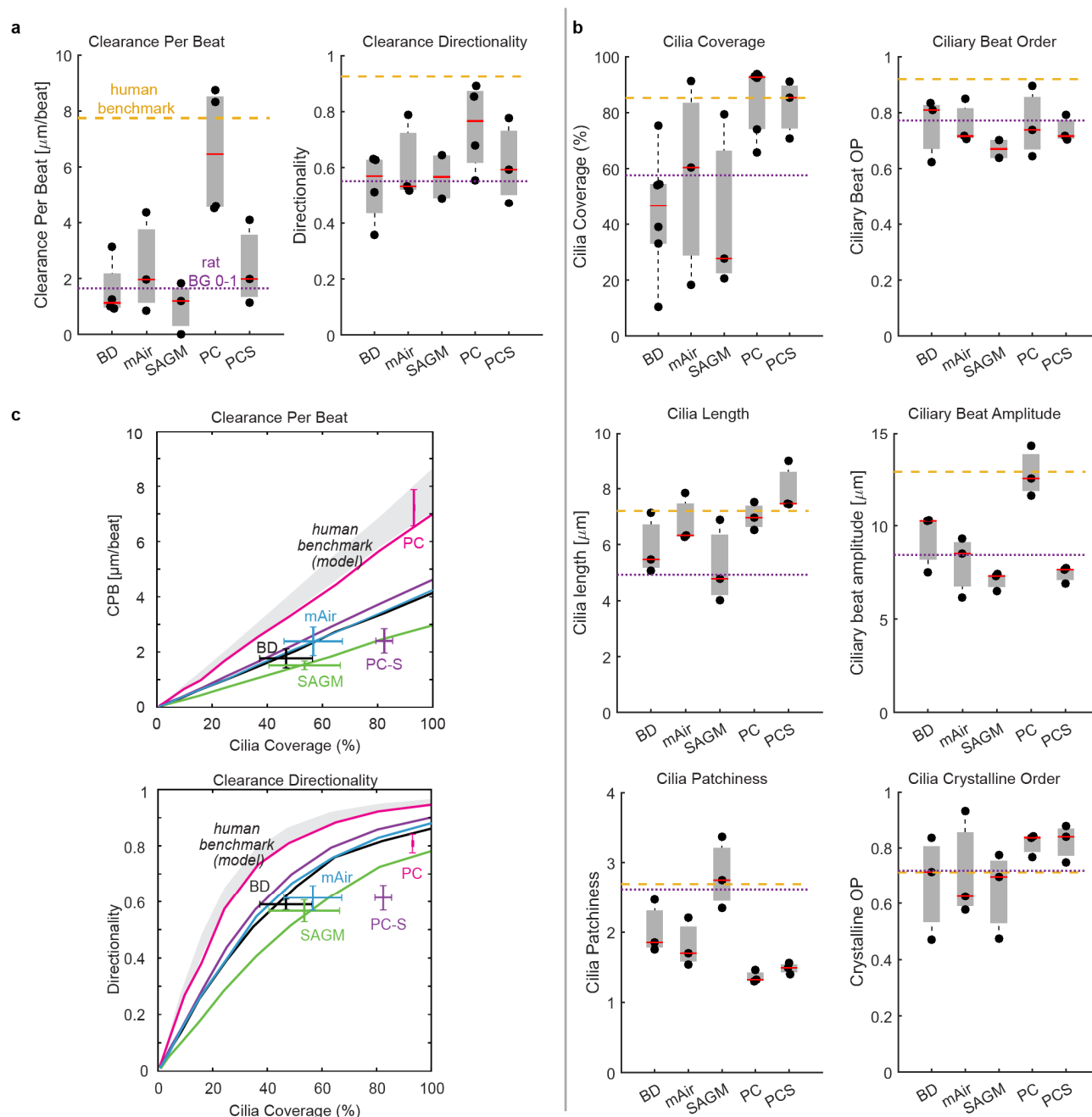
Figure 3: Quantitative analysis of ciliary beat parameters and their impact on clearance function.
a, Average cilia coverage, ciliary beat order, cilia patchiness, cilia crystalline order, cilia length, and ciliary beat amplitude measured in human BG0-6 and rat BG0-1. Solid dots are mean values of each donor (across multiple BGs), red line is median of distribution; significance was assessed with Kruskal–Wallis test. b, Schematic of ciliary input metrics on cell- and tissue-level used to predict output metrics of tissue-level clearance using physics-based computational model. c, Predicted clearance per beat and clearance directionality in human (red, BG 0-6) and rat (blue, BG 0-1). Solid line is mean prediction, shaded line is uncertainty based on spread of input metrics. Black data points represent experimental human benchmark and rat BG0-1 data (mean +/- SEM) indicating a good match of the model predictions.
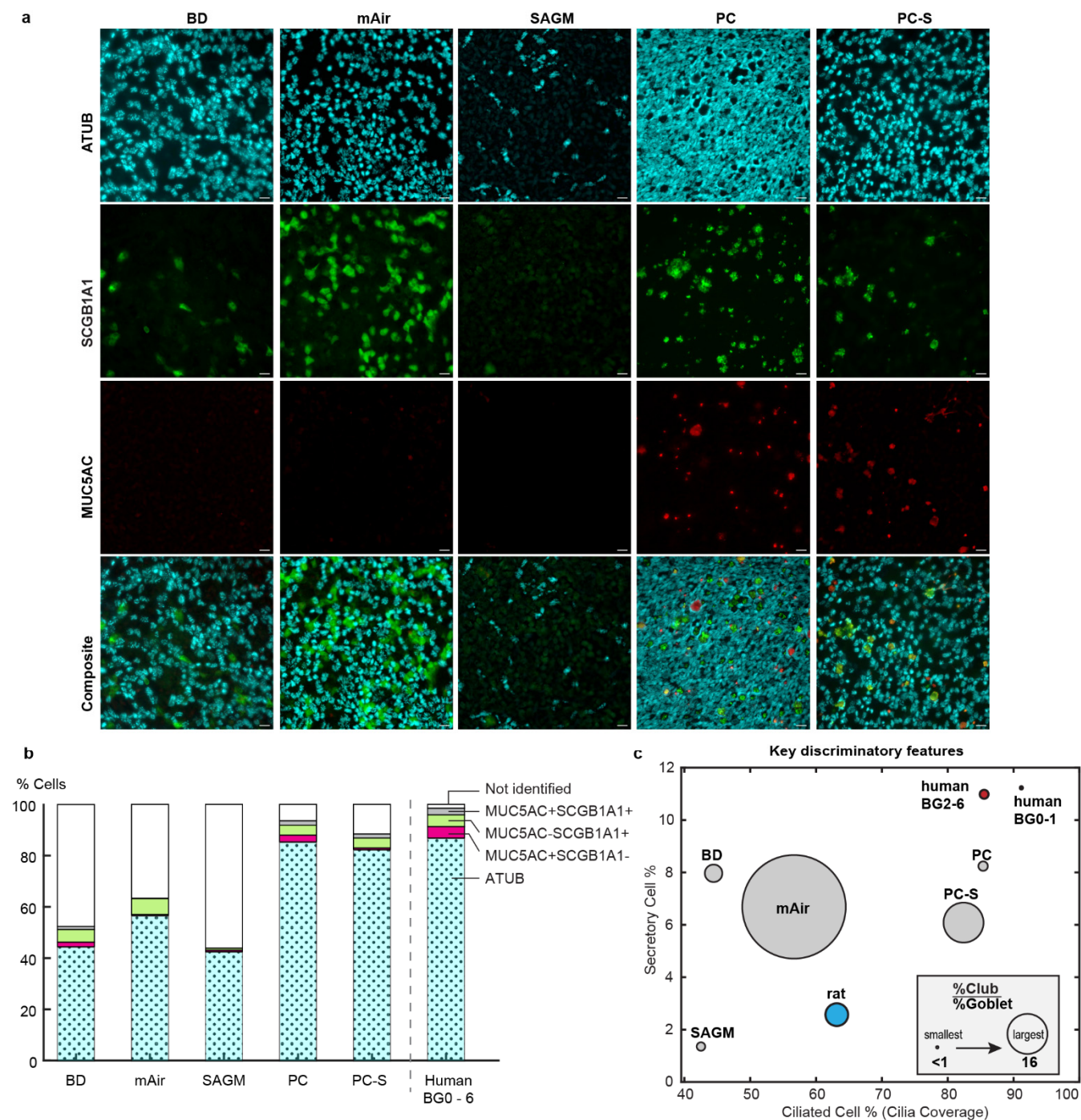
Figure 4: Impact of cell culture media on luminal cell type composition of pHAEC cultures. a, Representative IF-images of pHAEC cultures from 1 donor differentiated in different cell culture media for 28 days at ALI and stained for cilia (ATUB) and secretory cell markers (SCGB1A1, MUC5AC). b, Mean luminal cell type composition based on IF-staining across donors. c, Mapping of IF-staining data of *in vitro* and ex vitro samples onto three dimensions: % secretory cells (MUC5AC+ and/or SCGB1A1+),

% ciliated cells (cilia coverage; ATUB+ cells), and ratio of MUC5AC-SCGB1A1+ (Club cell) to MUC5AC+ SCGB1A1- (goblet cells) percentages.

Figure 5: Impact of cell culture media on ciliary beat and clearance function in pHAEC cultures. a, Quantitative analysis of particle CPB and directionality in pHAEC cultured in different differentiation media for 28 days at ALI compared to human benchmark and rat (BG0-1) data. b, Quantitative analysis of ciliary beat metrics in pHAEC cultured as in (a). Solid dots are mean of each donor (across multiple BGs), red line is median of distribution. c, Predicted CPB and clearance directionality in different pHAEC cultures compared to predicted human airway performance (grey shade). Data points indicate the particle clearance metrics experimentally measured in each medium (mean +/- SEM).
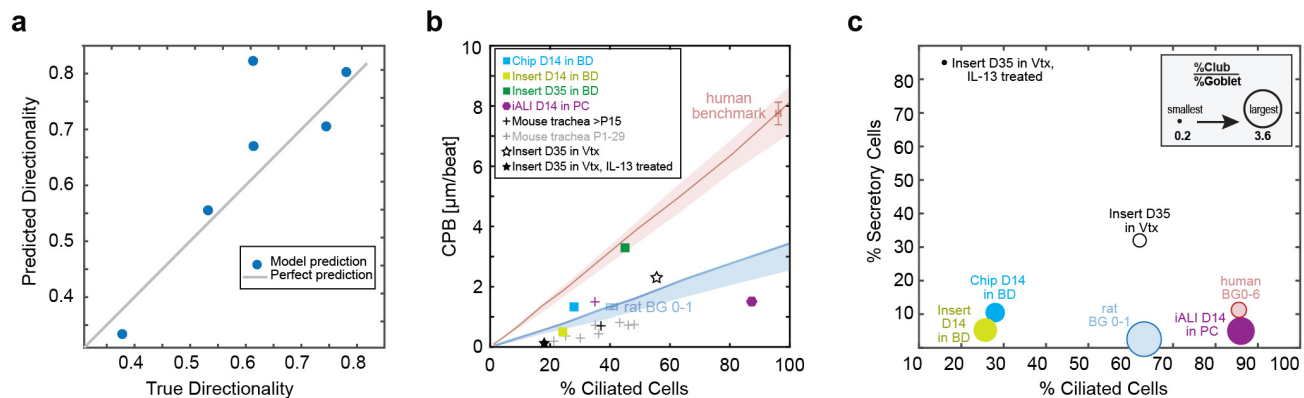
Figure 6: Phenotypic benchmarking using structural and functional maps of human mucociliary machinery. a, Linear regression model predicting clearance directionality in human airways using as input percentage of secretory cells, percentage of ciliated cells, and the ratio of club to goblet cell proportions. b, CPB map data comparing different human in vitro and rodent ex vivo models to human and rat benchmark curves. D, day at ALI; P, postnatal day; Vtx, Vertex ALI medium; iALI, human iPSC-derived differentiated airway epithelium. Red line and shaded region: Human model predictions; Blue line and shaded region: rat BG0-1 model predictions. c, Cellular composition map comparing different human in vitro models to human and rat benchmarks.